Photonic RF Synthesizer Based on a Phase-Locked Optoelectronic Oscillator Using Anti-Stokes Loss Spectrum of Stimulated Brillouin Scattering

Huanfa Peng, *Member, IEEE*, Peng Lei, Xiaopeng Xie, *Member, IEEE*, and Zhangyuan Chen, *Member, IEEE*

***Abstract*—Accurate, and low phase noise RF synthesis is crucial for various applications. The phase-locked loop (PLL) is the common architecture to synthesize high spectral purity RF carriers with desired frequencies. However, the phase noise is limited by the electrical voltage-controlled oscillators (VCOs). Optoelectronic oscillator (OEO) is an alternative of RF oscillator that allows overcoming the phase noise limitation of electrical oscillator. Here, we propose a novel photonic RF synthesizer by using a voltage-controlled optically tunable OEO as VCO in a PLL. By phase-locking OEO to a tunable RF reference, tunable RF carrier with precise frequency can be synthesized. The OEO incorporates a RF photonic filter as the mode selector harnessing the light-sound interaction in a fiber, namely the stimulated Brillouin scattering. Due to the low dissipation rate of the confined acoustic wave, a narrowband anti-Stokes loss spectrum is formed, which can be transformed into a high quality factor tunable RF bandpass filter with the aid of a phase modulated optical probe wave. It facilitates the removal of the supermodes and enables the frequency tuning of OEO. Experimentally, we attain a RF synthesizer with frequency synthesis tuning range from 6 GHz to 12 GHz. The minimum tuning step is 8 Hz. At 8.4 GHz, the phase noise is −125 dBc/Hz at 10 kHz offset. The phase-locking dynamics, frequency tunability, and phase noise are thoroughly investigated. Our approach offers the prospects of low phase noise RF synthesis with wide frequency range.**

***Index Terms*—Photonic RF synthesizer, phase-locking, optoelectronic oscillator, stimulated Brillouin scattering.**

I. Introduction

LOW phase noise and accurate RF synthesis is of great importance for a wide variety of demanding applications, such as radar, communication, instrumentation, sensing and metrology. A phase-locked loop (PLL) based RF synthesizer is the most common architecture to synthesize a series of RF carriers with desired frequencies owing to its high spectral purity, high frequency accuracy and wide frequency tuning range [1]. A generic PLL based RF synthesizer is comprised of a frequency stable reference, a phase detector, a loop filter, a RF frequency divider and an electrical voltage-controlled oscillator (VCO) [1]. Theoretically, the phase noise of the synthesized RF signal at the carrier offset beyond the PLL loop bandwidth is limited by the phase noise of the electrical VCO [1]. To synthesize ultra-high spectral purity RF signals with high carrier frequencies, a substantial challenge arises from the fact that the phase noise performance of the electrical VCOs deteriorate with the increase of the carrier frequency [2], which leads to the phase noise degradation of the synthesized RF signals. Alternatively, a hybrid optoelectronic oscillator (OEO) is a promising microwave oscillator that would enable high spectral purity RF signal generation due to the unique property of the phase noise is independent of oscillation frequency [3]. The OEOs use low loss optical fibers, optical waveguides or optical microcavities as the resonators in the oscillation loop, which shows higher quality factor than that of the electrical counterparts. To harness an OEO as the VCO in a PLL based RF synthesizer, the OEO should be capable of voltage-controlled frequency tuning. Essentially, the fine frequency tuning of the OEO can be attained by changing the loop length, while the coarse frequency tuning relies on the center frequency tuning of the mode selector in the OEO loop. The mode selector is intending to remove the supermodes induced by the long cavity of the OEO. A tunable electrical bandpass RF filter can be used as the tunable mode selector of the OEO to achieve the wideband frequency tuning [4], but with the issue of the broadening of the passband bandwidth of the RF filter at high frequency.

Recently, the wide frequency tuning of the OEO can be achieved via the incorporation of the RF photonic filters in the OEO loop [5]–[10]. Due to the appealing features of wide frequency tuning range, narrow passband and nearly no broadening of the passband bandwidth of the RF photonic filters, it permits us to achieve the OEOs with unprecedented fundamental oscillation frequency tuning range. In our preliminary work [9], [10], we exploited the stimulated Brillouin scattering (SBS) effect mediated by the nonlinear light-sound interaction in an optical fiber to attain the frequency tunable narrow passband mode selector in the OEO loop. Two types of wideband frequency tunable OEO by harnessing the narrowband Stokes gain spectrum and the anti-Stokes loss spectrum are respectively demonstrated, which featuring fundamental oscillation frequency tuning range as wide as 60 GHz with the use of SBS gain spectrum [9]. In particular, due to the mitigation of the transduction of the laser phase noise to the RF phase noise, the OEO by leveraging anti-Stokes

Manuscript received April 11, 2022; revised May 6, 2022; accepted May 10, 2022. Date of publication May 13, 2022; date of current version June 3, 2022. This work was supported in part by the National Natural Science Foundation of China under Grants 61805003 and 61690194. *(Corresponding author: Huanfa Peng.)*

The authors are with the State Key Laboratory of Advanced Optical Communication Systems and Networks, Department of Electronics, Peking University, Beijing 100871, China (e-mail: hf.peng@pku.edu.cn; leipengeecs@pku.edu.cn; xiaopeng.xie@pku.edu.cn; chenzhy@pku.edu.cn).

Digital Object Identifier 10.1109/JPHOT.2022.3174921

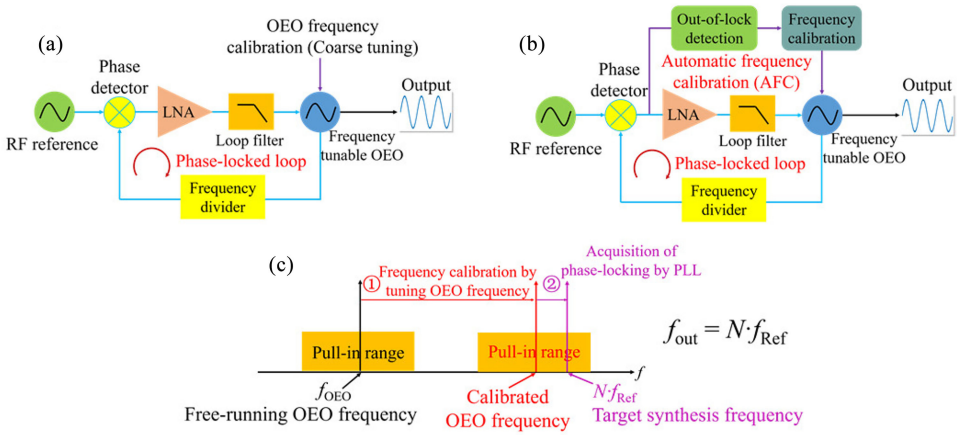

Fig. 1. System architectures of the PLL based photonic RF synthesizer by using an OEO as the VCO and the working principle of the phase-locking acquisition of the PLL. (a) With open loop frequency calibration for the phase-locking acquisition. (b) With automatic frequency calibration (AFC) system for the phase-locking acquisition. (c) Working principle of the frequency synthesis. LNA: low noise amplifier. N is the frequency division factor of the RF frequency divider, f_{Ref} is the frequency of the electrical reference, f_{OEO} is the frequency of the free-running OEO, f_{out} is the frequency of the synthesized RF signal.

loss spectrum of SBS is amenable to a higher spectral purity, frequency tunable RF oscillator [10]. Despite the remarkable progress of the wideband frequency tunable OEO by using RF photonic filters, the application of these wideband frequency tunable OEO in a RF frequency synthesizer system still remain unexplored. From the practical point of view, due to the potential prospects of high frequency accuracy, deterministic frequency output, low phase noise and high long-term stability offered by the RF synthesis technique, it is promising to unlock the potential advantages of the OEO in the practical applications. Although, the OEOs have been proposed to be used to develop wideband RF frequency synthesizers [11]–[13], the mode selectors in the OEO loop still rely on the electrical bandpass filters, which may limit the performance of the oscillation mode selection of the high frequency OEO [13].

In this paper, for the first time, we propose to use a voltage-controlled optically tunable OEO to implement a PLL based photonic RF synthesizer, which aims to attain ultra-low phase noise RF synthesis. In our scheme, the optically tunable OEO is used as the VCO in the PLL, which utilizes the anti-Stokes loss spectrum of SBS in a fiber to achieve the OEO oscillation mode selection and the voltage-controlled wideband frequency tunability. A voltage-controlled RF phase shifter is incorporated in the OEO loop to obtain the voltage-controlled continuous frequency tuning, which is demanded for the phase-locking of the OEO to a stable electrical reference via the PLL. To acquire the phase-locking for different target synthesis frequencies, the frequency of the OEO is coarsely calibrated by electrically controlling the wavelength difference between the co-propagating probe wave in the forward direction and pump wave in the backward direction within a same fiber. By precisely tuning the frequency of the electrical reference, a series of RF signals with different carrier frequencies can be synthesized. Experimentally, we attain a photonic RF synthesizer with a frequency synthesis tuning range from 6 GHz to 12 GHz. The minimum tuning step is 8 Hz. At 8.4 GHz, the phase noise can reach as low as -125 dBc/Hz at 10 kHz offset. The phase-locking dynamics, frequency tunability, and phase noise performance of our proposed system are thoroughly investigated. Compared with the free-running SBS based OEOs [9], [10], our proposed scheme offers the prospects of the RF signal generation with deterministic frequency output, higher long-term stability, higher frequency accuracy and higher frequency tuning resolution, which are beneficial for the practical applications [1].

II. System Architecture and Working Principle

A. Architectures of RF Synthesizer by Using an OEO as VCO

Fig. 1 shows the system architectures and working principle of our proposed PLL based photonic RF synthesizer. The PLL is comprised of a highly stable electrical reference, a phase detector, a low noise amplifier, a loop filter, a frequency tunable OEO, and a RF frequency divider. Essentially, the frequency tunable OEO is used as the VCO in the PLL. The aim of the PLL is to lock the frequency of the OEO to the integer multiples of the frequency of the electrical reference, which leads to a synthesized RF signal with the frequency of $N \cdot f_{\mathrm{Ref}}$. The N is the frequency division factor of the RF frequency divider, f_{Ref} is the electrical reference frequency. The RF frequency divider is intending to lower the frequency of the electrical reference. Moreover, the frequency of the electrical reference can be precisely changed. By tuning the electrical reference frequency, a series of RF signals with different RF frequencies can be synthesized. The most challenge of the system is the phase-locking acquisition of the PLL [14], which arises from the narrow continuous frequency tuning range of the OEO [15]. A narrow continuous frequency tuning range of the OEO leads to a narrow pull-in range of the PLL, which is unfavorable for the self-acquisition of the phase-locking. Hence, the frequency of the OEO should be coarsely calibrated to assist the phase-locking acquisition.

Here, we propose two methods to achieve phase-locking acquisition, as shown in Fig. 1(a) and (b). One is the open loop OEO frequency calibration, the other utilizes the automatic frequency

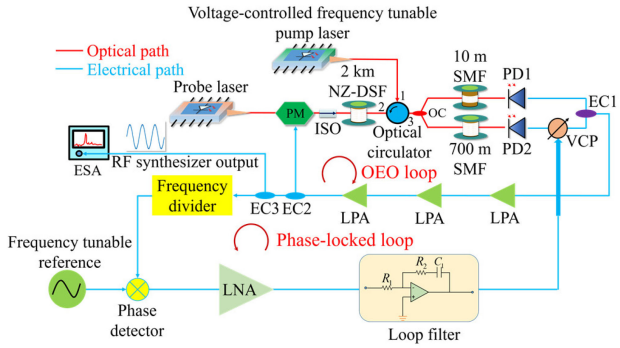

Fig. 2. Experimental setup. PM: phase modulator. ISO: optical isolator. OC: optical coupler. NZ-DSF: none-zero dispersion shifted fiber. SMF: single-mode fiber. PD1, PD2: photodiodes. VCP: voltage-controlled RF phase shifter. EC1, EC2, EC3: electrical couplers. LPA: low phase noise amplifier. LNA: low noise amplifier. ESA: electrical spectrum analyzer.

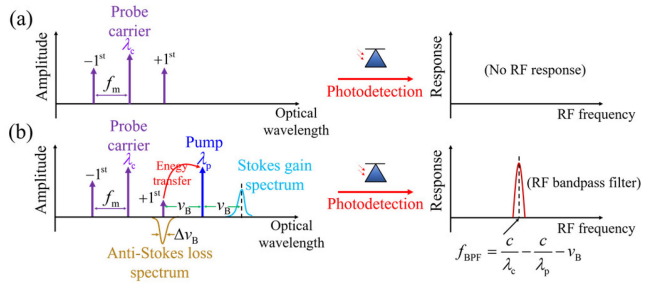

Fig. 3. Principle of the tunable RF photonic filter harnessing the SBS effect in a fiber. The forward is the phase modulated probe wave. The backward is the continuous-wave pump wave. $c, f_{\mathrm{m}}, \lambda_{\mathrm{c}}, \lambda_{\mathrm{p}}, \nu_{\mathrm{B}}, \Delta\nu_{\mathrm{B}}, f_{\mathrm{BPF}}$ denote the velocity of light in vacuum, RF modulation frequency, probe carrier wavelength, pump laser wavelength, Brillouin frequency shift, 3-dB bandwidth of the SBS anti-Stokes loss spectrum, and the center frequency of the RF photonic filter. (a) The photodetection of a phase modulated probe wave. (b) The $+1^{\mathrm{st}}$ order phase modulated sideband falls on the anti-Stokes loss spectrum of the SBS.

calibration (AFC) technique. The open loop calibration system relies on the open loop frequency tuning of the OEO, while the AFC method can automatically calibrate the frequency of the OEO to acquire the phase-locking. The AFC system can detect the locking state of the PLL with an out-of-lock detection unit, and automatically tune the frequency of OEO to make the target synthesis frequency fall in the pull-in range of the PLL. The AFC system has been proposed in our preliminary work to acquire phase-locking of a phase-locked OEO system to realize highly stable single frequency RF source, which shows robust, high speed and fully automatic operation [15]. The principle of the phase-locking acquisition of these two methods can be illustrated by Fig. 1(c). If the target synthesis frequency is out of the pull-in range of the PLL, the PLL is unable to achieve self-acquisition of the phase-locking. In this manner, the frequency of the OEO will be coarsely tuned to make it approach to the target synthesis frequency by the open loop calibration system or the AFC system, as shown by step 1. Once the target synthesis frequency falls in the pull-in range of the PLL, the OEO can be rapidly synchronized to the electrical reference, which leads to a synthesized RF signal with a precise frequency of $N{\cdot}f_{\mathrm{Ref}}$, which is indicated by step 2. By varying the frequency of the reference, a series of synthesized RF carriers can be attained.

B. Implementation of RF Synthesizer Based on a Phase-Locked Tunable OEO Harnessing Anti-Stokes Loss Spectrum of SBS

To implement the proposed photonic RF synthesizer shown in Fig. 1, an experiment is carried out. Here, we use the open loop calibration method shown in Fig. 1(a) to acquire the phase-locking of the PLL in our experiment. Fig. 2 shows the experimental setup of our RF frequency synthesizer. The system consists of two parts, which are the frequency tunable OEO based on the anti-Stokes loss spectrum of SBS and the PLL. The OEO is used as the VCO in the PLL. To stimulate the SBS in the fiber, we use a continuous-wave (CW) laser (Teraxion Inc., NLL) as the probe laser, and a voltage-controlled frequency tunable continuous-wave fiber laser (NKT photonics Inc.) as the pump laser. The frequency of the pump laser can be thermally tuned within 1 nm range and finely tuned by changing the voltage of the applied DC signal on the piezoelectric transducer (PZT). The probe laser is phase modulated by an electro-optic (EO) phase modulator (Eospace Inc.). The phase modulated optical probe wave is injected to a spool of 2 km non-zero dispersion shifted fiber (NZ-DSF) in the forward direction. Meanwhile, the light emitted from the pump laser is sent to the same fiber in the backward direction via an optical circulator. With an optical coupler, the light from the output of the port-3 of the optical circulator is split to two optical signals. The two optical signals are sent to two single-mode fiber links with fiber length of 10 meters and 700 meters, respectively. The output optical signals of the two fiber links are photodetected by two high speed photodiodes (PD1, PD2, APIC Inc.), respectively. The two photodetected RF signals are combined by an electrical coupler (EC1). Three low phase noise amplifiers (LPA, Analog Devices Inc., HMC-C072) with frequency response range from 6 GHz to 12 GHz are cascaded to amplify the combined RF signal. The amplified RF signal is fed back to drive the phase modulator. The use of two single-mode fiber links is intending to form a dual-loop OEO structure to further suppress the supermodes of the OEO. Note that a voltage-controlled RF phase shifter (VCP) is inserted to the long fiber link to realize the continuous frequency tuning of the OEO. The coarse frequency tuning of the OEO relies on the center frequency tuning of the photonic RF filter by leveraging the anti-Stokes loss spectrum of SBS.

Fig. 3 shows the working principle of the tunable RF photonic filter used in the OEO loop. The phase modulated probe wave and the continuous-wave pump wave are co-propagating in opposite directions in the fiber. The two first order sidebands of the phase modulated probe wave have anti-phases and equal amplitudes. No RF signals can be detected via the photodetection of the phase modulated probe wave due to the destructive interference of the two RF beat notes mediated by the beating of the carrier and the two phase modulated sidebands of the probe wave, as illustrated in Fig. 3(a). However, by introducing a backward pump wave in the fiber, as shown in Fig. 3(b), it can excite waveguide confined acoustic waves, which leads to the SBS process. The nonlinear SBS process strictly relies on the phase-matching condition [16].

Provided that the frequency difference of the pump wave and the $+1^{st}$ order phase modulated sideband of the probe wave satisfies:

$$f_{+1} - f_{\mathrm{p}} = \upsilon_{\mathrm{B}} \tag{1}$$

where f_{+1}, f_{p} and ν_{B} are the frequency of the $+1^{st}$ order phase modulated sideband of the probe wave, the pump wave frequency and the Brillouin frequency shift, respectively, the SBS process will occur. Under this case, the optical interference between the forward propagating phase modulated $+1^{st}$ order sideband of the probe wave and the backward propagating pump wave will excite moving acoustic wave in the fiber via the electrostriction effect, which can scatter the photons of the forward phase modulated $+1^{st}$ order optical sideband to the backward direction. The energy of the backscattered light will be coherently transferred to the pump wave, which forms a narrowband anti-Stokes loss spectrum. The phase modulated $+1^{st}$ order sideband falls on the SBS loss spectrum, which will significantly attenuate its optical power. Due to the low energy dissipation rate of the confined acoustic waves, the 3-dB bandwidth of the anti-Stokes loss spectrum can be as narrow as tens of MHz. After transferring the optical energy of the forward propagating phase modulated $+1^{st}$ order sideband to the backward propagating pump wave, it leads to asymmetrical optical sidebands of the forward propagating probe wave, which breaks the condition of the destructive interference of the RF beat notes in the former case. After the photodetection of the probe wave with asymmetrical optical sidebands via a fast photodiode, the optical notch filter formed by the SBS anti-Stokes loss spectrum can be transformed into a RF bandpass filter with passband bandwidth as narrow as tens of MHz, which facilitates the single oscillation mode selection of the OEO. By varying the frequency of the pump wave, the frequency of the passband of the tunable RF photonic filter will be changed, as shown by the formula of the center frequency f_{BPF} shown in Fig. 3(b), which will lead to the oscillation frequency tuning of the OEO. Here, we adjust the voltage of the applied DC signal on the PZT of the pump laser to rapidly change the frequency of the OEO. It provides the strategy for the frequency calibration of the OEO to achieve the PLL phase-locking acquisition. To lock the phase of OEO to the electrical reference (Keysight Inc., E8257D), a portion of the output of the OEO is frequency divided by a RF frequency divider (Analog Devices Inc., HMC862A). The frequency division factor of the RF frequency divider is 8. A phase detector formed by a double-balanced mixer (DBM) is utilized to convert the phase difference between the frequency tunable reference and the output of the RF frequency divider to an error signal. The error signal is amplified by a home-made low noise amplifier (LNA, Analog Devices Inc., OP27). Afterwards, the amplified error signal is fed back to drive the voltage-controlled RF phase shifter (VCP, CONNPHY Inc., CVPS-6G15G-360) after passing through a home-made second order proportional-integral (PI) loop filter.

III. Experimental Results and Discussions

To attain high selectivity of the oscillation mode of the OEO, a narrow passband of the photonic RF filter is favorable. Due to the SBS Stokes gain spectrum and anti-Stokes loss spectrum are influenced by the material properties and waveguide geometry of the optical fibers [17], the passband of the photonic RF filters by using different optical fibers are tested via a vector network analyzer (VNA, Keysight N5247A). Fig. 4(a) shows the passband responses at the center frequency of 8 GHz by using different kinds of fibers as the medium for SBS. A highly-nonlinear fiber (HNLF), a standard single-mode fiber (SMF), a dispersion shifted fiber (DSF), and a NZ-DSF are tested. Among them, by using NZ-DSF, it can achieve the smallest 3-dB bandwidth as narrow as 40 MHz. Note that the passband response presents multiple peaks, which originate from the interactions of the optical fundamental mode and multi-mode acoustic modes supported by the fiber [17]. With the use of SMF, it shows higher side peaks around the dominant passband peak, which is unfavorable for the oscillation mode selection in the OEO loop. Besides, Fig. 4(b) shows the 3-dB bandwidth of the passband as a function of the pump laser power for different fibers. The pump power is varied from 3 dBm to 15 dBm. With the increasing of the pump power, the 3-dB bandwidth of the passband by using NZ-DSF nearly keeps below those of the other fibers. Hence, we use the NZ-DSF as the medium for SBS in our OEO loop to attain higher OEO supermodes suppression.

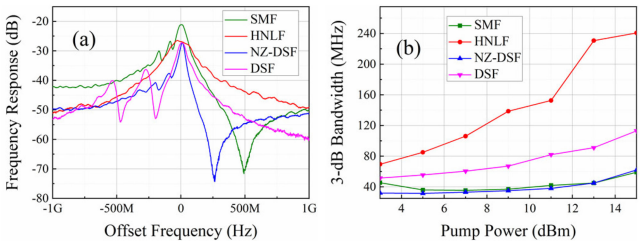

Fig. 4. Measured frequency response of the RF photonic filter based on the SBS anti-Stokes loss spectrum. (a) Comparison of the frequency responses with different kinds of optical fibers. The center passband frequencies are around 8 GHz. (b) The measured 3-dB bandwidth of the passband as a function of the power of the pump wave.

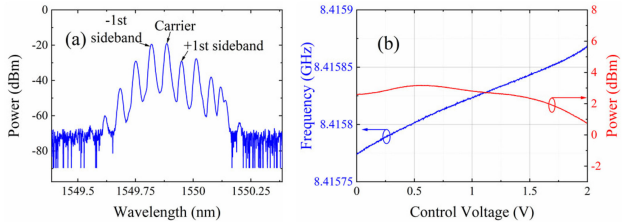

Fig. 5. (a) Optical spectrum of the output signal of the port-3 of the optical circulator. (b) The characteristics of the OEO frequency and RF power as a function of the DC bias voltage of the VCP.

Fig. 5(a) shows the optical spectrum of the optical signal at the output of the port-3 of the optical circulator when the oscillation frequency of the OEO is around 8.4 GHz. The wavelength of the pump laser is located in the right side of the $+1^{st}$ order phase modulated sideband of the probe wave. The Brillouin frequency shift is estimated to be 10.7 GHz. Besides, the power of the $+1^{st}$ order phase modulated sideband is suppressed by more than 10 dB due to the transfer of its

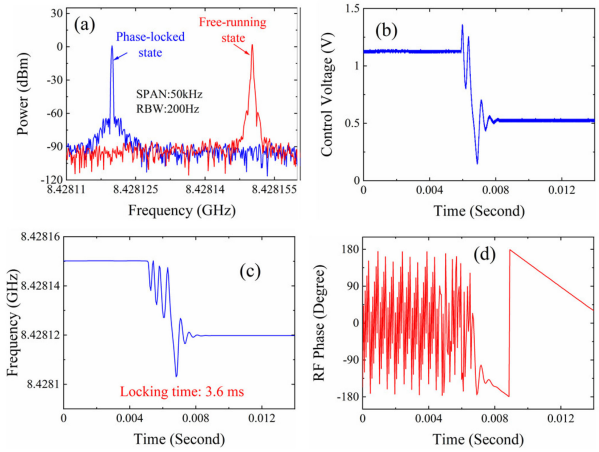

Fig. 6. (a) The measured electrical spectra of the free-running and the phase-locked OEOs. (b) Transient response of the feedback error signal during the process of phase-locking. (c) Transient response of the RF frequency change. (d) Transient response of the RF phase change.

energy to the backward propagating pump wave, which results in asymmetrical modulation sidebands. It should be worth noted that the phase modulation sidebands up to the $\pm 3^{rd}$ orders exist due to the large modulation depth of the phase modulation. Through the power ratio of the -1^{st} order sideband and the carrier in Fig. 5(a), the phase modulation depth can be extracted to be around 1.4. The large phase modulation depth is attained due to the high saturation power of the low phase noise amplifier and the ultra-low half-wave voltage of the phase modulator. A large phase modulation depth is intended to improve the power of the $+1^{st}$ order sideband, which enhances the optical interference of the forward $+1^{st}$ phase modulated sideband and the backward pump wave. A stronger optical interference is beneficial for the initiation of SBS effect through the electrostriction [18], which facilitates the oscillation mode selection of the OEO. Besides, the voltage-controlled continuous frequency tuning of the OEO is also characterized, as presented in Fig. 5(b). The blue curve shows the characteristics of the OEO frequency by varying the DC bias voltage of the VCP in the OEO loop. The bias voltage of the VCP varies from 0 V to 2 V. Besides, the red curve indicates the RF power of the OEO as a function of the DC bias voltage of the VCP. It should be noted that the oscillation frequency of the OEO is quasi-linearly increased. The frequency increment is around 100 kHz. Correspondingly, the voltage-controlled frequency sensitivity of the OEO is estimated to be 50 kHz/V. Besides, the variation of the RF power is below 2 dB. A small RF power variation is favorable for the phase-locking.

To make a comparison of the RF spectrum purity of the free-running OEO and the phase-locked OEO, the RF spectra of these two states are measured by an electrical spectrum analyzer (ESA, Keysight N9030A) with the same span and resolution bandwidth (RBW), as shown in Fig. 6(a). In the free-running state, the oscillation RF signal features higher close-in carrier noise due to the influences of the thermal fluctuation and environmental vibration on the OEO, as indicated by the red curve. In contrast, by phase-locking the OEO to the electrical reference, the close-in carrier noise of the synthesized RF tone is significantly suppressed, as shown by the blue curve. It indicates the PLL can assist the OEO to against the effects of the thermal noise and environmental vibration. Furthermore, to investigate the dynamics of the phase-locking acquisition of the PLL, the transient responses of the feedback error signal of the PLL, RF frequency and RF phase of the OEO are measured by a signal source analyzer (SSA, Keysight E5052B+E5053A), as shown in Fig. 6(b)–(d), respectively. To acquire the phase-locking, we coarsely calibrate the frequency of the OEO by changing the voltage of the applied DC signal on the PZT of the pump laser. Once the frequency difference of the free-running OEO and the target synthesis frequency is smaller than the pull-in range of the PLL, it will lead to the phase-locking acquisition of the PLL. During the phase-locking process, the voltage of the feedback error signal, and the OEO frequency experience damped oscillations and finally converge to the steady states, which indicates the frequency of the OEO is locked to the integer multiples of the frequency of the electrical reference. Moreover, the abrupt phase change occurs during the phase-locking process, as shown in Fig. 6(d). The phase-locking time is estimated to be 3.6 ms, which can be further reduced by increasing the loop gain of the PLL. For instance, by increasing the voltage gain of the LNA in the PLL loop, the phase-locking speed can be faster. Note that the temperature variations on the system will lead to the frequency drift of the free-running OEO. If the frequency drift of the OEO exceeds the pull-in range of the PLL, it will result in the out of lock of the PLL [15]. As analyzed in our previous work [10], under the influence of the temperature variations, the frequency drift of the SBS based OEO is mainly induced by two mechanisms. The first one is that the thermal expansion and thermal refractive index change of the fiber will degrade the frequency stability of the OEO. Typically, the thermal frequency stability of the free-running fiber based OEO is expected to be 8 ppm/K [19], [20]. To prevent the out of lock of the PLL, the fiber spools should be thermally stabilized [19]. The second mechanism is that the thermal laser frequency drifts of the probe laser and pump laser will induce the RF phase delay fluctuations of the SBS based RF photonic filter in the OEO loop, which results in the frequency drift of the OEO [10]. To guarantee small frequency fluctuations of the lasers, the temperature of the probe laser and pump laser modules are stabilized by the built-in temperature control systems.

To investigate the wide frequency tunability of the proposed RF frequency synthesizer, the electrical reference frequency is changed, which leads to different target locking frequencies. Correspondingly, by changing the voltage of the applied DC signal on the PZT of the tunable pump laser, it can lead to the acquisition of the phase-locking at different target locking frequencies. The maximum voltage-controlled frequency tuning range of the pump laser is tested to be around 8 GHz. Fig. 7(a) shows the superposition of the electrical spectra of the synthesized RF carriers with different RF frequencies. The frequency synthesis tuning range is from 6 GHz to 12 GHz with a coarse frequency tuning step around 250 MHz. The frequency tuning range is limited by the frequency response range of the low phase noise amplifiers, which can be further improved by using a pump laser with wider voltage-controlled

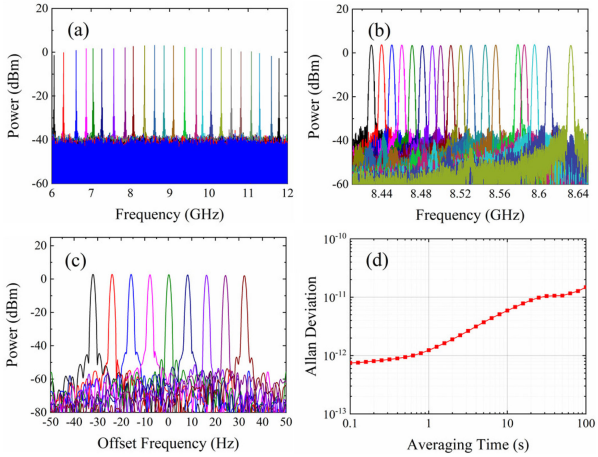

Fig. 7. Tunable electrical spectra and frequency stability. (a) Tunable electrical spectra from 6 GHz to 12 GHz. (b) Tunable electrical spectra from 8.4 GHz to 8.6 GHz. (c) Fine frequency synthesis with 8 Hz tuning step. The carrier frequency is around 8.4 GHz. (d) The measured Allan deviation of the synthesized RF signal with frequency of 8.4 GHz.

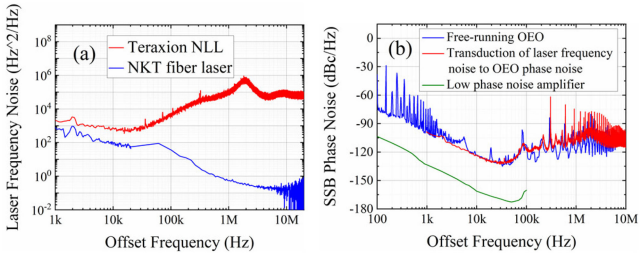

Fig. 8. (a) The measured laser frequency noise spectra of the probe laser and the pump laser used in our experiments. (b) SSB phase noise of the 8.4 GHz free-running OEO (blue), the experimentally predicted OEO phase noise (red) and the phase noise induced by the low phase noise amplifiers (olive). The predicted phase noise curve takes into account the transduction of the laser frequency noise to the OEO phase noise.

frequency tuning range and broadband RF amplifiers. Fig. 7(b) exhibits the frequency synthesis tuning spectra from 8.4 GHz to 8.6 GHz with a medium frequency tuning step around 10 MHz. Note that the medium frequency tuning step is not uniform, which attributes to the Vernier effect of the dual fiber loop of the OEO [21]. Moreover, by tuning the frequency of the reference with a step of 1 Hz, the frequency of the synthesizer can be precisely varied with a step of 8 Hz, as shown in Fig. 7(c), which indicates the frequency of our proposed RF synthesizer can be precisely tuned. Moreover, to investigate the long-term frequency stability of the proposed RF synthesizer, the Allan deviation of the synthesized 8.4 GHz signal is shown in Fig. 7(d). The averaging time is from 0.1 s to 100 s. At the averaging time of 100 s, the Allan deviation is measured to be 1.5×10^{-11}. Theoretically, the long-term frequency stability of our proposed RF synthesizer is determined by the frequency stability of the electrical reference. By using a reference with higher long-term stability, the frequency stability of the proposed RF synthesizer can be further increased.

The phase noise of the OEO is of crucial for the performance of the PLL based RF synthesizer. As demonstrated in our preliminary work [10], the origin of the phase noise limitation of the SBS based OEOs are dominated by the frequency noise of the probe and pump lasers. According to the Kramers-Kronig relation, the introduce of the anti-Stokes loss spectrum in the fiber will lead to the small change of the refractive index within the SBS loss spectrum [17]. In this manner, the phase modulated $+1^{st}$ order sideband falls on the loss spectrum will experience a SBS induced optical phase shift. In the presence of the laser frequency fluctuations of the probe and pump lasers, it results in the SBS induced optical phase fluctuations imposed to the phase modulated $+1^{st}$ order sideband, which decorrelates the optical phase between the probe carrier and the phase modulated $+1^{st}$ order sideband. After the photodetection of the probe wave with asymmetrical sidebands, the laser frequency noise of the pump laser and probe laser will be transduced to the phase noise of the OEO. To experimentally investigate the conversion of the laser frequency noise to the RF phase noise of the OEO, the frequency noise spectra of the probe laser and pump laser are measured by an optical noise analyzer (SYCATUS Inc., A0040A), as shown in Fig. 8(a). The Fourier offset frequency range is from 1 kHz to 20 MHz. The frequency noise of the pump laser is much lower than that of the probe laser. It should be noted that the frequency noise spectrum of the NKT fiber laser in the offset frequency range from 20 kHz to 20 MHz is measured by the high sensitivity mode of the optical noise analyzer due to the ultra-narrow linewidth of the NKT fiber laser. Moreover, the phase noise of the 8.4 GHz free-running OEO is measured, as shown by the blue curve in Fig. 8(b). Theoretically, the contribution of the SBS induced laser frequency noise to the OEO phase noise can be predicted by multiplying the sum of the laser frequency noise of the two lasers with the dual-loop transfer function of the OEO and a conversion factor [10]. Given a conversion factor of -158.8 dB, it shows high correlation between the predicted phase noise curve and the measured phase noise curve, as the comparison of the red and blue curves in Fig. 8(a). To quantitatively determine the conversion factor in theory, as derived by our preliminary work [10], the conversion factor of the SBS induced laser frequency noise to the OEO phase noise is:

$$F_C = \left(\frac{1}{L-1}\frac{\ln L}{\Delta v_B}\right)^2 \tag{2}$$

where L is the amplitude loss of the $+1^{st}$ order sideband. According to the measured optical spectrum shown in Fig. 5(a) and the passband bandwidth of the SBS based RF photonic filter shown in Fig. 4(b), the amplitude loss of the $+1^{st}$ order sideband and the 3-dB bandwidth of the SBS anti-Stokes loss spectrum are around 3.2 and 40 MHz, respectively. By substituting these parameters into (2), the conversion factor of the laser frequency noise to OEO phase noise is calculated to be -157.6 dB, which indicates an excellent agreement between the theoretically calculated conversion factor and the experimentally predicted conversion factor. Note that the raise of the phase noise floor of the OEO within the offset frequency range from 100 kHz to 10 MHz attributes to the high frequency noise floor of the probe laser (Teraxion Inc., NLL). By using a probe laser with lower frequency

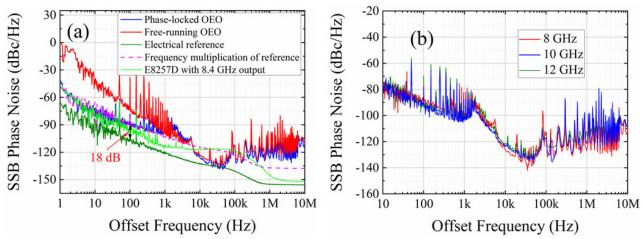

Fig. 9. (a) SSB phase noise of the 1.05 GHz electrical reference, the 8.4 GHz free-running OEO, the 8.4 GHz phase-locked OEO, and a commercial benchtop RF synthesizer. The magenta dashed line is the predicted phase noise of the frequency multiplication of the 1.05 GHz reference. (b) SSB phase noise of the synthesized RF signals with different RF frequencies.

noise floor, the phase noise floor of the OEO is predicted to be optimized. Moreover, the phase noise contribution of the low phase noise amplifiers to the OEO is estimated by multiplying the additive phase noise of the low phase noise amplifiers with the transfer function of the dual-loop OEO [10], as illustrated by the olive curve in Fig. 8(b). It indicates that the phase noise contribution of the low phase noise amplifiers is predicted to be lower than the phase noise transduction of the laser frequency noise.

To make a comparison of the phase noise of the electrical reference, the free-running OEO and the phase-locked OEO, we measured the SSB phase noise of the 1.05 GHz reference, 8.4 GHz free-running OEO, 8.4 GHz phase-locked OEO, as shown in Fig. 9(a). The loop bandwidth of the PLL is around 2 kHz. Within the loop bandwidth, the phase noise of the phase-locked OEO is strongly suppressed when compared with the free-running OEO. Theoretically, the phase noise of the phase-locked OEO within the PLL loop bandwidth is determined by the phase noise of the electrical reference. As the frequency of the OEO is locked to the 8 times of the electrical reference frequency, it raises the phase noise of the electrical reference by $20\times\log_{10}(8) \approx 18$ dB to the phase noise of the 8.4 GHz phase-locked OEO. It should be worth noted that the noise of the PLL circuits can also contribute to the synthesized RF signal via the feedback control loop [22]. For instance, the flicker noise of the LNA in the PLL can be transferred to the phase noise of the synthesized RF signal. Theoretically, based on the phase noise transfer function of the PLL phase noise model, the phase noise contribution of the LNA can be derived as $S_{\varphi}(f) \approx (N/K_{\mathrm{pd}})^2 S_{\mathrm{n}}(f)$ at low offset frequency range [13]. f is the Fourier offset frequency, N is the frequency division factor of the RF frequency divider, K_{pd} is the phase detector gain, and $S_{\mathrm{n}}(f)$ is the power spectral density of the LNA voltage noise. In our case, N is 8 and K_{pd} is measured to be around 0.5 rad/V. According to the specifications of the LNA with the model of OP27 (Analog Devices Inc.), the power spectral density of the flicker noise is -166 dBV^2/Hz. To the end, the phase noise contribution of the LNA flicker noise is estimated to be -142 dBc/Hz at 1 Hz offset, which is below the phase noise contribution of the reference oscillator. Beyond the loop bandwidth, the PLL has no phase correction to the OEO, which results in the phase noise of the phase-locked OEO inherits that of the free-running OEO. The phase noise of the synthesized RF signal can be as low as -125 dBc/Hz at 10 kHz offset. Note that there are some spurs at integer multiples of 50 Hz, which are induced by the interference of the laser power supply. It should be worth noted that the PLL features a relative small loop bandwidth, which is intending to optimize the overall phase noise performance of the synthesized RF signal. Since the phase noise of the reference oscillator will contribute to the synthesized RF signal within the PLL loop bandwidth, we predicted the phase noise curve of the frequency multiplication of the reference, as illustrated by the magenta dashed line in Fig. 9(a). It indicates that the free-running OEO features lower phase noise than that of the frequency multiplication of the reference at offset frequency above 5 kHz. To avoid high phase noise contribution of the reference oscillator to the synthesized RF signal at offset above 5 kHz, we choose the intersection point of the phase noise curve of the free-running OEO (red) and the predicted phase noise contribution curve of the reference oscillator (magenta) as the PLL loop bandwidth. The offset frequency of the intersection point is around 2 kHz. However, a relative small loop bandwidth will lead to a slow phase-locking process, as indicated by the milliseconds lock-in time shown in Fig. 6(c). Moreover, a phase noise comparison between a commercial benchtop RF synthesizer (Keysight Inc., E8257D) and our proposed system is carried out, as shown by the blue curve and the green curve. Within the offset frequency range from 7 kHz to 90 kHz, the phase noise performance of our proposed synthesizer is better than that of the benchtop RF synthesizer. Besides, to make a comparison of the phase noise performance of the synthesized RF signals with different RF frequencies, the phase noise of three synthesized RF signals with frequencies around 8 GHz, 10 GHz and 12 GHz are measured, as shown in Fig. 9(b). Phase noise variations exist among different RF frequencies. At 10 kHz offset, the maximum phase noise variation is around 3 dB. Within the PLL loop bandwidth, the experimental phase noise for different synthesized RF signals show tiny difference. Theoretically, if the phase noise contribution of the reference oscillator dominates, the phase noise of the RF synthesizer will increase at higher frequency due to the phase noise degradation of the electrical reference oscillator. Beyond the loop bandwidth, in principle, the phase noise of the OEO is nearly independent of the oscillation frequency provided that the additive phase noise of the OEO loop is invariant within a wide oscillation frequency range [3]. However, for a practical implementation of the OEO, at higher oscillation frequency range, the phase noise performance of the OEO may slightly degrade due to the higher additive phase noise of the OEO loop [10].

IV. Conclusion

In summary, a PLL based photonic RF synthesizer based on a phase-locked optically tunable OEO is proposed and experimentally demonstrated. The incorporation of the tunable RF photonic filter utilizing the anti-Stokes loss spectrum of SBS in the OEO loop enables the voltage-controlled wide frequency tuning of the OEO, which provides the strategy of the PLL phase-locking acquisition at different synthesis frequencies via the wideband frequency calibration of the OEO. Due to the

mitigation of the transduction of laser phase noise to the RF phase noise of the SBS anti-Stokes loss spectrum based RF photonic filter, the voltage-controlled frequency tunable OEO features phase noise as low as −125 dBc/Hz at 10 kHz offset, which facilitates low phase noise of the RF synthesizer. Our approach can benefit from the OEO's characteristics of the low phase noise and the phase noise is nearly independent of oscillation frequency, which permits us to attain a high frequency RF synthesizer with ultra-low phase noise and without phase noise degradation in a wide synthetic frequency range. Besides, with the potential of the fully integrated SBS based OEO in a nanophotonic platform [23], our proposed system is amenable to a chip-scale photonic RF synthesizer through the integration of the PLL circuits and the photonic integrated SBS based OEO.

REFERENCES

[1] A. Chenakin, "Frequency synthesis: Current status and future projections," *Microw. J.*, vol. 60, no. 4, pp. 22–36, Apr. 2017.

[2] A. P. S. Khanna, "Microwave oscillators: The state of the technology," *Microw. J.*, vol. 49, no. 4, pp. 22–28, Apr. 2006.

[3] L. Maleki, "Sources: The optoelectronic oscillator," *Nature Photon.*, vol. 5, pp. 728–730, 2011.

[4] D. Eliyahu and L. Maleki, "Tunable, ultra-low phase noise YIG based opto-electronic oscillator," in *Proc. IEEE MTT-S Int. Microw. Symp. Dig.*, 2003, vol. 3, pp. 2185–2187.

[5] A. A. Savchenkov *et al.*, "Voltage-controlled photonic oscillator," *Opt. Lett.*, vol. 35, no. 10, pp. 1572–1574, May 2010.

[6] W. Li and J. Yao, "An optically tunable optoelectronic oscillator," *J. Lightw. Technol.*, vol. 28, no. 18, pp. 2640–2645, Sep. 2010.

[7] D. Eliyahu *et al.*, "Resonant widely tunable opto-electronic oscillator," *IEEE Photon. Technol. Lett.*, vol. 25, no. 15, pp. 1535–1538, Aug. 2013.

[8] X. Xie *et al.*, "Wideband tunable optoelectronic oscillator based on a phase modulator and a tunable optical filter," *Opt. Lett.*, vol. 38, no. 5, pp. 655–657, 2013.

[9] H. Peng *et al.*, "Tunable DC-60 GHz RF generation utilizing a dual-loop optoelectronic oscillator based on stimulated Brillouin scattering," *J. Lightw. Technol.*, vol. 33, no. 13, pp. 2707–2715, Jul. 2015.

[10] H. Peng *et al.*, "Wideband tunable optoelectronic oscillator based on the deamplification of stimulated Brillouin scattering," *Opt. Exp.*, vol. 25, no. 9, pp. 10287–10305, 2017.

[11] T. Sun, L. Zhang, and A. S. Daryoush, "High-resolution *X*-Band frequency synthesizer using SILPLL optoelectronic oscillators," *IEEE Trans. Ultrasonics, Ferroelect., Freq. Control*, vol. 67, no. 1, pp. 217–223, Jan. 2020.

[12] H. Chen, I. A. Ukaegbu, B. Nakarmi, and S. Pan, "RF multiplier based on harmonic-locked SMFP-LD and OEO structure," *IEEE Access*, vol. 10, pp. 435–440, Dec. 2022.

[13] H. Peng, N. Liu, X. Xie, and Z. Chen, "Photonic microwave synthesizer based on optically referenced sub-sampling phase-locked optoelectronic oscillator," *Opt. Commun.*, vol. 499, 2021, Art. no. 127304.

[14] F. M. Gardner, *Phaselock Techniques*. Hoboken, NJ, USA: Wiley, 2005, pp. 183–203.

[15] H. Peng, N. Liu, X. Xie, and Z. Chen, "Fast automatic frequency calibration assisted phase-locked highly stable optoelectronic oscillator," *Opt. Exp.*, vol. 29, no. 4, pp. 6220–6235, Feb. 2021.

[16] M. G. Herraez, K. Y. Song, and L. Thevenaz, "Optically controlled slow and fast light in optical fibers using stimulated Brillouin scattering," *Appl. Phys. Lett.*, vol. 87, no. 8, 2005, Art. no. 081113.

[17] G. P. Agrawal, *Nonlinear Fiber Optics*. Waltham, MA, USA: Academic, 2013, pp. 353–391.

[18] A. Kobyakov, M. Sauer, and D. Chowdhury, "Stimulated Brillouin scattering in optical fibers," *Adv. Opt. Photon.*, vol. 2, no. 1, pp. 1–59, 2010.

[19] D. Eliyahu, K. Sariri, M. Kamran, and M. Tokhmakhian, "Improving short and long term frequency stability of the opto-electronic oscillator," in *Proc. IEEE Int. Freq. Control Symp. PDA Exhib.*, 2002, pp. 580–583.

[20] M. Kaba *et al.*, "Improving thermal stability of opto-electronic oscillators," *IEEE Microw. Mag.*, vol. 7, no. 4, pp. 38–47, Aug. 2006.

[21] X. S. Yao and L. Maleki, "Multi-loop optoelectronic oscillator," *IEEE J. Quantum Electron.*, vol. 36, no. 1, pp. 79–84, Jan. 2000.

[22] D. H. Wolaver, *Phase-Locked Loop Circuit Design*. Englewood Cliffs, NJ, USA: Prentice-Hall, 1991, pp. 107–129.

[23] M. Merklein *et al.*, "Widely tunable, low phase noise microwave source based on a photonic chip," *Opt. Lett.*, vol. 41, no. 20, pp. 4633–4636, Oct. 2016.